Nodeless Variables Finite Element Method and Adaptive Meshing Teghnique for Viscous Flow Analysis

Archawa Paweenawat, Pramote Dechaumphai*

Mechanical Engineering Department, Chulalongkorn University,
Bangkok 10330, Thailand

A nodeless variables finite element method for analysis of two-dimensional, steady-state viscous incompressible flow is presented. The finite element equations are derived from the governing Navier-Stokes differential equations and a corresponding computer program is developed. The proposed method is evaluated by solving the examples of the lubricant flow in journal bearing and the flow in the lid-driven cavity. An adaptive meshing technique is incorporated to improve the solution accuracy and, at the same time, to reduce the analysis computational time. The efficiency of the combined adaptive meshing technique and the nodeless variables finite element method is illustrated by using the example of the flow past two fences in a channel.

Key Words : Finite Element Method, Incompressible Flow, Nodeless Variables, Adaptive Meshing Technique

1. Introduction

The finite element method has been widely and successfully used as a tool for analyzing both the solid mechanics and heat transfer problems. However, its application in the field of fluid dynamics is still under development and is limited, because the method has encountered some difficulties arisen from the nature of the governing Navier-Stokes differential equations (Zienkiewicz and Taylor, 2000). This is mainly due to the fact that the derivative terms of the velocity components in the momentum equations are one order higher than those of the pressure. The order of the finite element interpolation functions for the velocity components is thus required to be one order higher than that of the pressure to assure the solution's stability (Patankar, 1980 ; Chen

* Corresponding Author,
  E-mail : fmepdc@eng.chula.ac.th
  TEL : +66-2-218-6621; **FAX** : +66-2-218-6621
  Mechanical Engineering Department, Chulalongkorn University, Bangkok 10330, Thailand. (Manuscript **Received** May 12, 2005; **Revised** July 2, 2006)
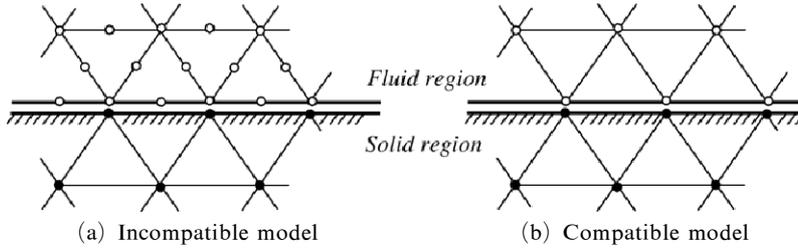
and Han, 2000 ; Schafer and Teschauer, 2001). In addition, the non-linearity nature of the Navier-Stokes equations also poses difficulty in the analysis. An iterative computational procedure is needed to obtain the flow solution. Solving such the fluid problems thus normally requires larger computer memory and computational time as compared to those for the solid mechanics and heat transfer problems.

In the past, the six-node triangular elements were generally employed for the low- speed viscous flow analysis in arbitrary two-dimensional geometry. The mixed element interpolation functions were selected such that the interpolation functions for the velocity components are one order higher than those for the pressure (Yamada et al., 1975 ; Kawahara et al., 1976). The use of the six-node elements requires extra effort for generating the finite element meshes and their related element data as compared to the regular three-node elements (Dechaumphai and Sikkhabandit, 2000). Furthermore, additional difficulty arises if both the fluid and the solid regions are to be solved together simultaneously as in the interdisciplinary problem (Wansophark et al., 2005). The finite

Fig. 1 Modeling incompatibility from using the six-node triangular elements in the fluid region for interdisciplinary fluid/solid problem

element modeling incompatibility occurs because the three-node triangular elements are normally used in the solid region, while the six-node elements are required in the fluid region for the fluid analysis as highlighted in Fig. 1(a). Development of an alternative finite element method for the flow analysis using the three-node triangular elements, as shown in Fig. 1(b) for fluid/solid modeling compatibility, is thus needed. Therefore, in this paper, the finite element method for the analysis of viscous incompressible flow using the regular three-node elements with nodeless variables is developed. The performance of the new finite element and the proposed method is evaluated by the analyzing several the viscous incompressible flow problems.

In addition, an adaptive meshing technique (Limtrakarn and Dechaumphai, 2004) is also implemented. The technique generates small clustered elements in the regions of high changes in solution gradients to improve solution accuracy. Larger elements are generated in the other regions where the solutions are fairly uniform to reduce the number of unknowns and thus the analysis computational time. The efficiency of the combined adaptive meshing technique and the nodeless variables finite element method is demonstrated by the problem of the flow past two fences in a channel.

2. Governing Equations

The governing differential equations for the viscous incompressible flow problems consist of the Navier-Stokes equations and the continuity equation. The two-dimensional steady-state Navier-Stokes equations, which represent the conservation of momentums in the x and y-directions, can be written as,

$$\rho\left(u\frac{\partial u}{\partial x}+v\frac{\partial u}{\partial y}\right)-\frac{\partial \sigma_x}{\partial x}-\frac{\partial \tau_{yx}}{\partial y}=0 \qquad (1a)$$

$$\rho\left(u\frac{\partial v}{\partial x}+v\frac{\partial v}{\partial y}\right)-\frac{\partial \tau_{xy}}{\partial x}-\frac{\partial \sigma_y}{\partial y}=0 \qquad (1b)$$

where ρ is the density : u and v are velocity components in the x and y-directions, respectively. For the Newtonian fluid, the normal and tangential stress components in Eqs. (1a) and (1b) above are written in terms of the pressure, p, and the velocity gradients as,

$$\sigma_x=-p+2\mu\frac{\partial u}{\partial x} \qquad (2a)$$

$$\sigma_y=-p+2\mu\frac{\partial v}{\partial y} \qquad (2b)$$

$$\tau_{xy}=\tau_{yx}=\mu\left(\frac{\partial u}{\partial y}+\frac{\partial v}{\partial x}\right) \qquad (2c)$$

where μ is the viscosity. The Navier-Stokes equations can then be rewritten in the form of nonlinear partial differential equations of second order as,

$$\rho\left(u\frac{\partial u}{\partial x}+v\frac{\partial u}{\partial y}\right)-\mu\left(\frac{\partial^2 u}{\partial x^2}+\frac{\partial^2 u}{\partial y^2}\right)+\frac{\partial p}{\partial x}=0 \quad (3a)$$

$$\rho\left(u\frac{\partial v}{\partial x}+v\frac{\partial v}{\partial y}\right)-\mu\left(\frac{\partial^2 v}{\partial x^2}+\frac{\partial^2 v}{\partial y^2}\right)+\frac{\partial p}{\partial y}=0 \quad (3b)$$

The above two equations, together with the continuity equation representing the conservation of mass,

$$\frac{\partial u}{\partial x}+\frac{\partial v}{\partial y}=0 \qquad (3c)$$

are to be solved for the unknowns of the velocity components and the pressure.

These differential equations, Eqs. (3a) ~ (3c), are to be solved with appropriate boundary conditions which are either specifying velocity components along edge S_1,

$$u(x, y) = u_1(x, y) \qquad (4a)$$

$$v(x, y) = v_1(x, y) \qquad (4b)$$

or surface tractions along edge S_2,

$$T_x = \sigma_x l + \tau_{xy} m \qquad (5a)$$

$$T_y = \tau_{xy} l + \sigma_y m \qquad (5b)$$

where l and m are the direction cosines of the unit vector normal to the boundary edge.

3. Finite Element Formulations

The Galerkin finite element method is applied for deriving the finite element equations from the governing differential equations, Eqs. (3a) ~ (3c). The computational domain is discretized using the regular three-node finite elements. These three-node finite elements assume the element velocity component and the pressure distributions in the form,

$$p(x, y) = H_i(x, y) p_i \qquad (6a)$$

$$u(x, y) = H_i(x, y) u_i' + G_j(x, y) u_j'' \qquad (6b)$$

$$v(x, y) = H_i(x, y) v_i' + G_j(x, y) v_j'' \qquad (6c)$$

where u_i' and v_i', $i = 1, 2, 3$, are the velocity components at the three nodes, and p_i is the nodal pressure. The u_j'' and v_j'', $j = 1, 2, 3$, are nodeless variables related to velocity components that do not need their locations as required by the actual nodes. The element interpolation functions, H_i, are linear in the form,

$$H_1 = L_1 \qquad (7a)$$

$$H_2 = L_2 \qquad (7b)$$
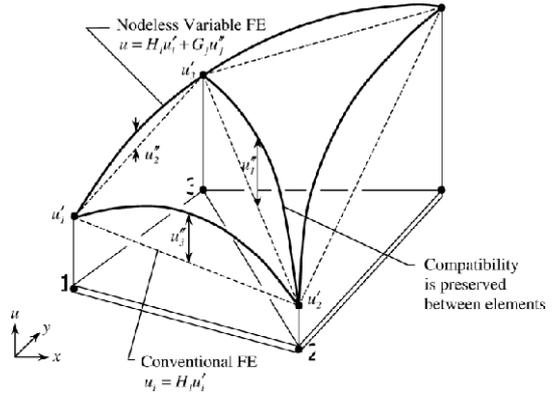
$$H_3 = L_3 \qquad (7c)$$

Fig. 2 Meaning and distribution of the nodeless variable finite elements with the preserved compatibility condition along element interface

and the nodeless variable interpolation functions, G_j, are quadratic in the form,

$$G_1 = 4L_2 L_3 \qquad (8a)$$

$$G_2 = 4L_1 L_3 \qquad (8b)$$

$$G_3 = 4L_1 L_2 \qquad (8c)$$

where L_i are the area coordinates (Zienkiewicz and Taylor, 2000). Distributions of these functions together with the nodeless variables as compared to those for the conventional 3-node element are shown in Fig. 2. The figure also shows that the compatibility condition is always preserved along the element interfaces to ensure the solution convergence. For simplicity in the derivation of the finite element equations presented later, the element velocity component distributions in Eqs. (6b) and (6c) are first written in the form,

$$u(x, y) = N_i(x, y) u_i \qquad (9a)$$

$$v(x, y) = N_i(x, y) v_i \qquad (9b)$$

where $i = 1$ to 6. The Bubnov-Galerkin finite element method is applied to the differential Eqs. (3a) ~ (3c) for deriving the finite element equations by using the element interpolation functions above. The finite element equations in form of integrals over the element domain A and the

element edge S_2 are,

$$\int_A N_i u\, u_{,x} dA + \int_A N_i v\, u_{,y} dA - \frac{1}{\rho}\int_A N_{i,x}p\,dA$$
$$+\frac{2\mu}{\rho}\int_A N_{i,x}u_{,x}dA + \frac{\mu}{\rho}\int_A N_{i,y}u_{,y}dA \qquad (10a)$$
$$+\frac{\mu}{\rho}\int_A N_{i,y}v_{,x}dA = \int_{S_2} N_i T_x dS$$

$$\int_A N_i u\, v_{,x} dA + \int_A N_i v\, v_{,y} dA - \frac{1}{\rho}\int_A N_{i,y}p\,dA$$
$$+\frac{\mu}{\rho}\int_A N_{i,x}u_{,y}dA + \frac{\mu}{\rho}\int_A N_{i,x}v_{,x}dA \qquad (10b)$$
$$+\frac{2}{\rho}\int_A N_{i,y}v_{,y}dA = \int_{S_2} N_i T_x dS$$

$$\int_A H_i(u_{,x}+v_{,y})\,dA = 0 \qquad (10c)$$

Then, by the substitution of Eqs. (9a) and (9b) into equations (10a) and (10b), the finite element equations can be written in form of the tensor notations as,

$$K_{\alpha\beta\gamma x}u_\beta u_\gamma + K_{\alpha\beta\gamma y}v_\beta u_\gamma - H_{\alpha\mu x}p_\mu$$
$$+S_{\alpha\beta xx}u_\beta + S_{\alpha\beta xy}v_\beta = Q_{\alpha x} \qquad (11a)$$

$$K_{\alpha\beta\gamma x}u_\beta u_\gamma + K_{\alpha\beta\gamma y}v_\beta v_\gamma - H_{\alpha\mu y}p_\mu$$
$$+S_{\alpha\beta yx}u_\beta + S_{\alpha\beta yy}v_\beta = Q_{\alpha y} \qquad (11b)$$

$$H_{\beta\mu x}u_\beta + H_{\beta\mu y}v_\beta = 0 \qquad (11c)$$

where the coefficients in these equations are defined by,

$$K_{\alpha\beta\gamma x}=\int_A N_\alpha N_\beta N_{\gamma,x}dA \qquad (12a)$$

$$K_{\alpha\beta\gamma y}=\int_A N_\alpha N_\beta N_{\gamma,y}dA \qquad (12b)$$

$$H_{\alpha\lambda x}=\frac{1}{\rho}\int_A N_{\alpha,x}H_\lambda dA \qquad (12c)$$

$$H_{\alpha\lambda y}=\frac{1}{\rho}\int_A N_{\alpha,y}H_\lambda dA \qquad (12d)$$

$$S_{\alpha\beta xx}=\frac{2\mu}{\rho}\int_A N_{\alpha,x}N_{\beta,x}dA + \frac{\mu}{\rho}\int_A N_{\alpha,y}N_{\beta,y}dA \quad (12e)$$

$$S_{\alpha\beta xy}=\frac{\mu}{\rho}\int_A N_{\alpha,y}N_{\beta,x}dA \qquad (12f)$$

$$S_{\alpha\beta yx}=\frac{\mu}{\rho}\int_A N_{\alpha,x}N_{\beta,y}dA \qquad (12g)$$

$$S_{\alpha\beta yy}=\frac{\mu}{\rho}\int_A N_{\alpha,x}N_{\beta,x}dA + \frac{2\mu}{\rho}\int_A N_{\alpha,y}N_{\beta,y}dA \quad (12h)$$

$$Q_{\alpha x}=\int_{S_2} N_i T_x dS \qquad (12i)$$

$$Q_{\alpha y}=\int_{S_2} N_i T_y dS \qquad (12j)$$

4. Computational Procedure

The finite element equations, as shown in Eqs. (11a) $\sim$ (11c) are non-linear to be solved by an iterative method. The Newton-Raphson iterative method is selected in this study. The method requires writing the unbalance values in the form,

$$F_{\alpha x}=K_{\alpha\beta\gamma x}u_\beta u_\gamma + K_{\alpha\beta\gamma y}v_\beta u_\gamma$$
$$-\frac{1}{\rho}H_{\alpha\lambda x}p_\lambda + S_{\alpha\beta xx}u_\beta + S_{\alpha\beta xy}v_\beta - Q_{\alpha x} \qquad (13a)$$

$$F_{\alpha y}=K_{\alpha\beta\gamma x}u_\beta v_\gamma + K_{\alpha\beta\gamma y}v_\beta v_\gamma$$
$$-\frac{1}{\rho}H_{\alpha\lambda y}p_\lambda + S_{\alpha\beta yx}u_\beta + S_{\alpha\beta yy}v_\beta - Q_{\alpha y} \qquad (13b)$$

$$F_\mu = H_{\beta\mu x}u_\beta + H_{\beta\mu y}v_\beta \qquad (13c)$$

Then application of the method leads to a set of algebraic equations with incremental unknowns in the form,

$$\begin{bmatrix} G_{\alpha\beta x} & L_{\alpha\beta y} & -H_{\alpha\lambda x} \\ L_{\alpha\beta x} & G_{\alpha\beta y} & -H_{\alpha\lambda y} \\ H_{\beta\mu x} & H_{\beta\mu y} & 0 \end{bmatrix} \begin{Bmatrix} \Delta u_\beta \\ \Delta v_\beta \\ \Delta p_\beta \end{Bmatrix} = \begin{Bmatrix} F_{\alpha x} \\ F_{\alpha y} \\ F_\mu \end{Bmatrix} \qquad (14)$$

where the coefficients in the above equations. are,

$$G_{\alpha\beta x}=K_{\alpha\beta\gamma x}u_\gamma + K_{\alpha\gamma\beta x}u_\gamma + K_{\alpha\gamma\beta y}v_y + S_{\alpha\beta xx} \quad (15a)$$

$$G_{\alpha\beta y}=K_{\alpha\beta\gamma y}v_\gamma + K_{\alpha\gamma\beta y}v_\gamma + K_{\alpha\gamma\beta x}u_y + S_{\alpha\beta yy} \quad (15b)$$

$$L_{\alpha\beta x}=K_{\alpha\beta\gamma x}v_\gamma + S_{\alpha\beta yx} \qquad (15c)$$

$$L_{\alpha\beta y}=K_{\alpha\beta\gamma y}u_\gamma + S_{\alpha\beta xy} \qquad (15d)$$

These coefficients which are in form of element matrices can be evaluated in closed-form ready for computer programming. Details of the derivation for these element matrices are omitted herein for brevity. In these Eqs. (15a) $\sim$ (15d), u_γ and v_γ

are the values of the velocity components for both the actual nodes and the nodeless variables at the ith iteration. The iteration process is terminated if the change in percentage of the overall errors of the nodal unknowns from the previous iteration is less than the specified value.

5. Adaptive Meshing Technique

The idea behind the adaptive meshing technique (Limtrakarn and Dechaumphai, 2004) presented herein is to construct a new mesh based on the solution obtained from the previous mesh. The new mesh will consist of small elements in the regions with large change in solution gradients and large elements in the other regions where the change in solution gradients is small. To determine proper element sizes at different locations in the flow field, the solid-mechanics concept for determining the principal stresses from a given state of stresses at a point is employed. Since small elements are needed in the regions of complex flow behavior, thus the velocity distribution can be used as an indicator in the determination of proper element sizes.

To determine proper element sizes, the second derivatives of the flow velocity with respect to the global coordinates x and y are first computed,

$$\begin{bmatrix} \dfrac{\partial^2 V}{\partial x^2} & \dfrac{\partial^2 V}{\partial x \partial y} \\ \dfrac{\partial^2 V}{\partial x \partial y} & \dfrac{\partial^2 V}{\partial y^2} \end{bmatrix} \qquad (16)$$

where V is the magnitude of the two velocity components u and v,

$$V = \sqrt{u^2 + v^2} \qquad (17)$$

The principal quantities in the principal directions X and Y where the cross derivatives vanish, are then determined,

$$\begin{bmatrix} \dfrac{\partial^2 V}{\partial X^2} & 0 \\ 0 & \dfrac{\partial^2 V}{\partial Y^2} \end{bmatrix} \qquad (18)$$

The magnitude of the larger principal quantity is

then selected,

$$\lambda = \max \left(\left| \frac{\partial^2 V}{\partial X^2} \right|, \left| \frac{\partial^2 V}{\partial Y^2} \right| \right) \qquad (19)$$

This value is used to compute proper element size h at that location from the conditions,

$$h^2 \lambda = \text{constant} = h_{\min}^2 \lambda_{\max} \qquad (20)$$

where $h_{\min}$ is the specified minimum element size, and $\lambda_{\max}$ is the maximum principal quantity for the entire model.

6. Examples

In this section, three examples are presented. The first two examples are used to verify and evaluate the nodeless variables finite element method with exact solution and solution from other numerical method. The third example is used to demonstrate the capability of the combined nodeless variable finite element method and the adaptive meshing technique to improve the analysis solution accuracy.

6.1 Lubricant flow in journal bearing

The problem statement of the lubricant flow in journal bearing is shown in Fig. 3. The problem can be simplified as illustrated in the Fig. 4 if the length L is much larger than the gap h. The figure shows the lower sliding pad moving at a velocity U relative to the stationary pad inclined
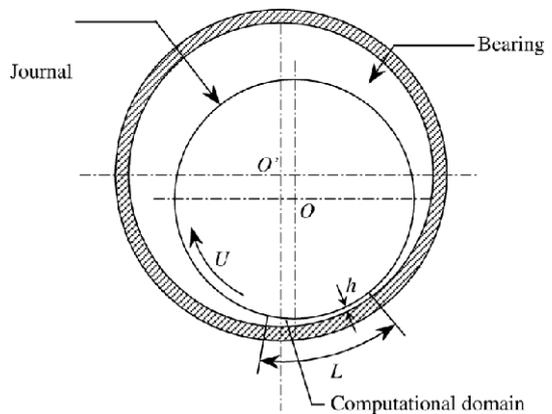

Fig. 3 Problem statement of lubricant flow in journal bearing

at a small angle with respect to the sliding pad. The small gap between the two pads is filled with a lubricant. The exact solution of the velocity is (Reddy and Gartling, 1994),

$$u = \frac{1}{2\mu} \frac{\partial p}{\partial x} y(y-h) + U\left(1 - \frac{y}{h}\right) \qquad (21)$$

where

$$h = h_0 + (h_L - h_0)\frac{x}{L} \qquad (22)$$

and the exact solution for the pressure distribution is,

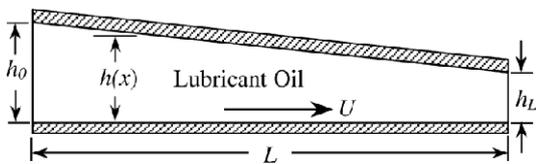$$\frac{P}{\mu UL/h_0^2} = \frac{6(x/L)(1-x/L)(1-h_L/h_0)}{(1+h_L/h_0)[1-(1-h_L/h_0)x/L]^2} \qquad (23)$$

Fig. 4 Computational domain for lubricant flow in journal bearing
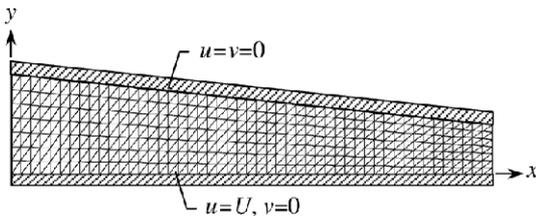
Fig. 5 Finite element model and boundary conditions of lubricant flow in journal bearing
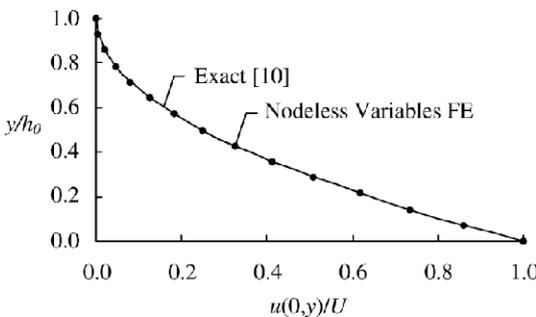
Fig. 6 Comparison of velocity profiles along the left boundary

In the computation, the values of $h_L = 2$, $h_0 = 1$, $L = 20$, $U = 5$, and $\mu = 10$ are selected. The finite element model as shown in Fig. 5 consists of 686 nodeless variables finite elements. Figures 6 and 7 show good agreement between the predicted and the exact solutions for the velocity profiles at the entrance and the exit of the computational domain. Figure 8 also shows good comparison of the predicted and the exact pressure distributions along the lower boundary of the computational model.

6.2 Lid-driven cavity flow

The problem of the flow circulation in a closed cavity driven by a moving lid has been widely used to validate new fluid computational methods. The problem statement is illustrated in Fig. 9. The flow circulation in a unit square cavity is induced by a moving lid at the velocity of $U = 1$ to the right. A finite element model, with a 50×50 mesh discretization along the x and y directions, consisting of all the nodeless variable finite
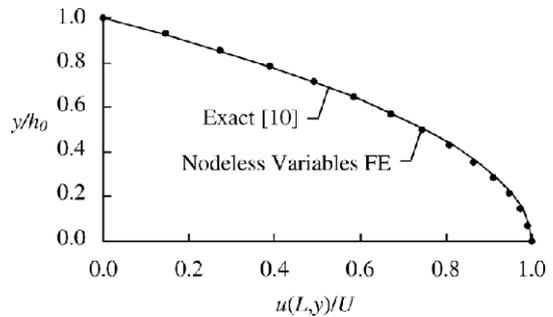

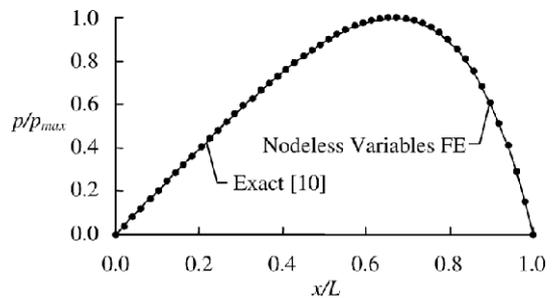**Fig. 7** Comparison of velocity profiles along the right boundary

Fig. 8 Comparison of pressure distributions along the bottom boundary

elements is shown in Fig. 10. The predicted velocity vectors of the flow circulation behavior at
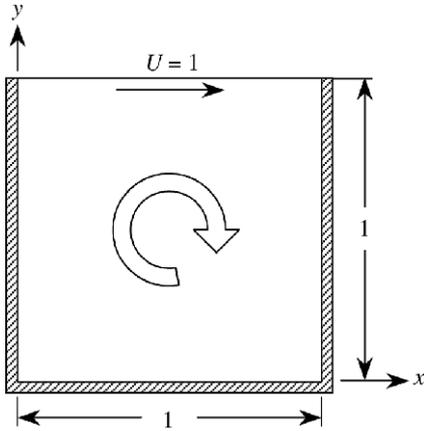

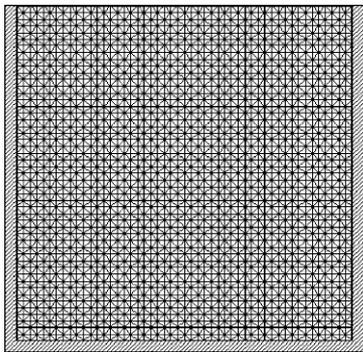Fig. 9   Problem statement of lid-driven cavity flow

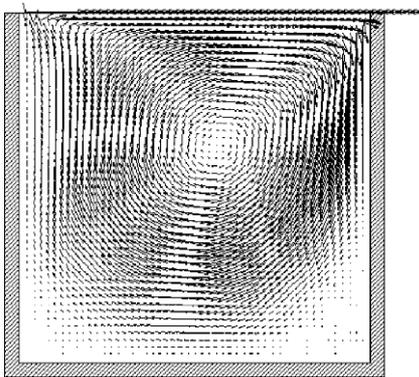Fig. 10   Finite element model of lid-driven cavity flow problem

Fig. 11   Predicted velocity vectors of lid-driven cavity flow problem

the Reynolds number of 400 are plotted in Fig. 11. Figure 12 shows good agreement of the velocity profiles along the cavity centered lines obtained from the nodeless variables finite element method and those presented Ref. (Ramaswamy and Jue, 1991).

6.3   Flow past two fences in channel

The problem of a flow past two fences in a channel is used to evaluate the performance of the combined nodeless variables finite element method and the adaptive meshing technique. The problem statement of the flow past the two fences in the channel with its geometry are shown in Fig. 13. Results of the flow behavior for this problem, including the separations behind the obstacles, were obtained by experiment and presented in Ref. (Durst et al., 1988).

The procedure of the combined nodeless variables finite element method and the adaptive meshing technique starts from generating a crude uniform mesh throughout the model as shown in Figs. 14(a) ∼ (c). The nodeless variables finite element method is then employed to predict the flow solution according to this first uniform mesh. The flow solution shown in Figs. 14(d) ∼ (f) is then used, based on the adaptive meshing technique described in Section 5, to construct a new mesh. This second mesh as shown in Figs. 15(a) ∼ (c) consists of clustered small elements in the regions of high changes in the solution gradients. Larger elements are, at the same time, generated in the other regions where the flow solution is fairly uniform. The nodeless variables finite ele-
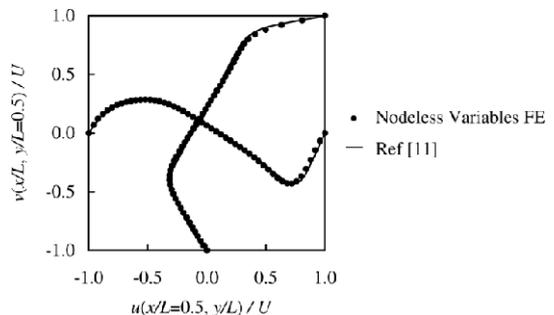

Fig. 12   Comparison of velocities of lid-driven cavity flow problem

ment method is then performed using this second mesh to produce a new flow solution as shown in Figs. 15(d) ~ (f). This procedure of generating new mesh and performing finite element computation is repeated. Figure 16(a) shows the third adaptive mesh. Small elements are clustered in the upper left corner of both the left and the right

fences, as shown in Figs. 16(b)-(c), where the fluid pressures change abruptly. The figure also shows that larger elements are generated in the other regions to reduce the computational time and the computer memory requirement.

Small elements generated at the upper left corners of both the fences provide high solution ac-
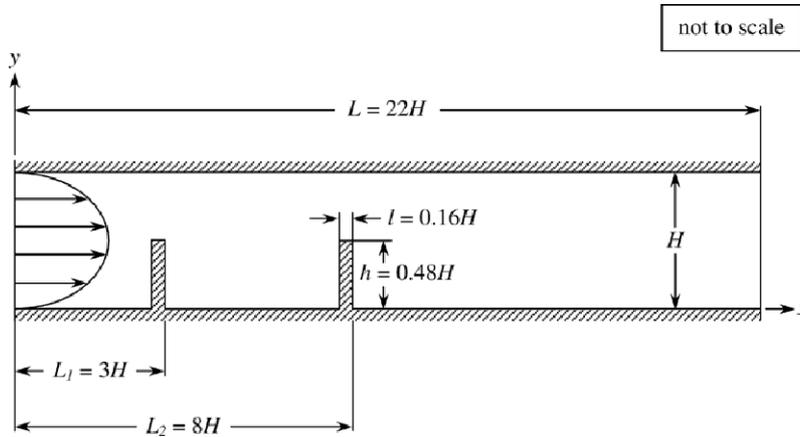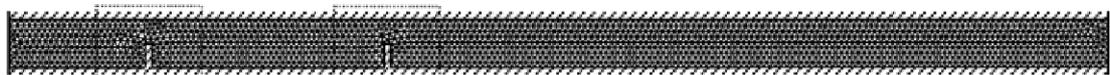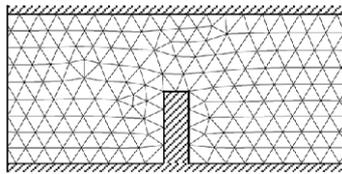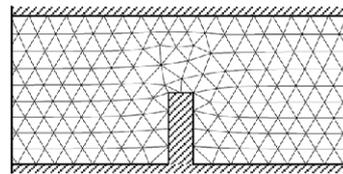

Fig. 13   Problem statement for flow past two fences in channel
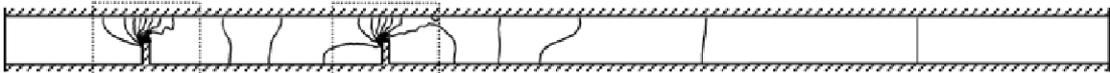

(a) First adaptive finite element mesh

(b) Detailed mesh around the left fence

(c) Detailed mesh around the right fence

(d) Predicted pressure distribution

(e) Detailed pressure distribution around the left fence

(f) Detailed pressure distribution around the right fence

Fig. 14   First adaptive mesh and its solution for flow past two fences in channel problem

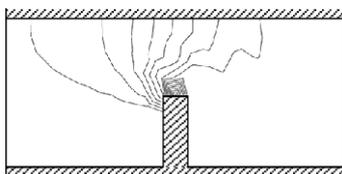(a) Second adaptive finite element mesh

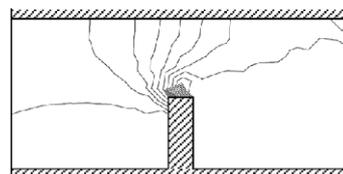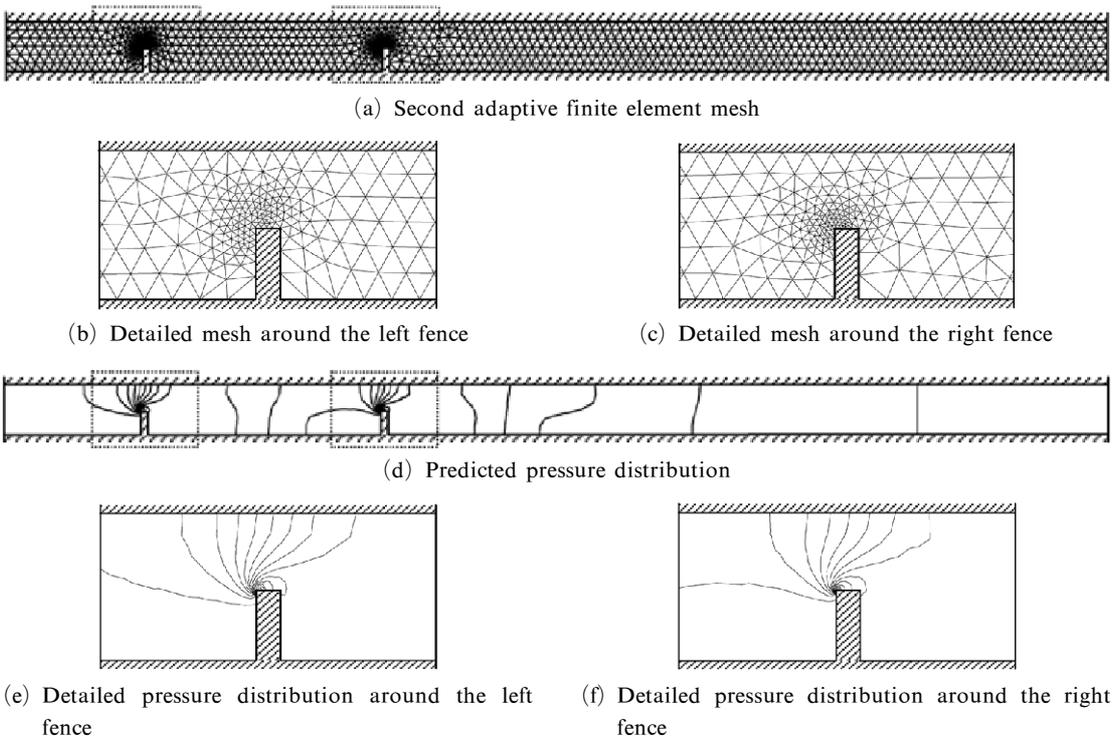(b) Detailed mesh around the left fence

(c) Detailed mesh around the right fence

(d) Predicted pressure distribution

(e) Detailed pressure distribution around the left fence

(f) Detailed pressure distribution around the right fence

Fig. 15   Second adaptive mesh and its solution for flow past two fences in channel problem

(a) Third adaptive finite element mesh

(b) Detailed mesh around the left fence

(c) Detailed mesh around the right fence

(d) Predicted pressure distribution

(e) Detailed pressure distribution around the left fence

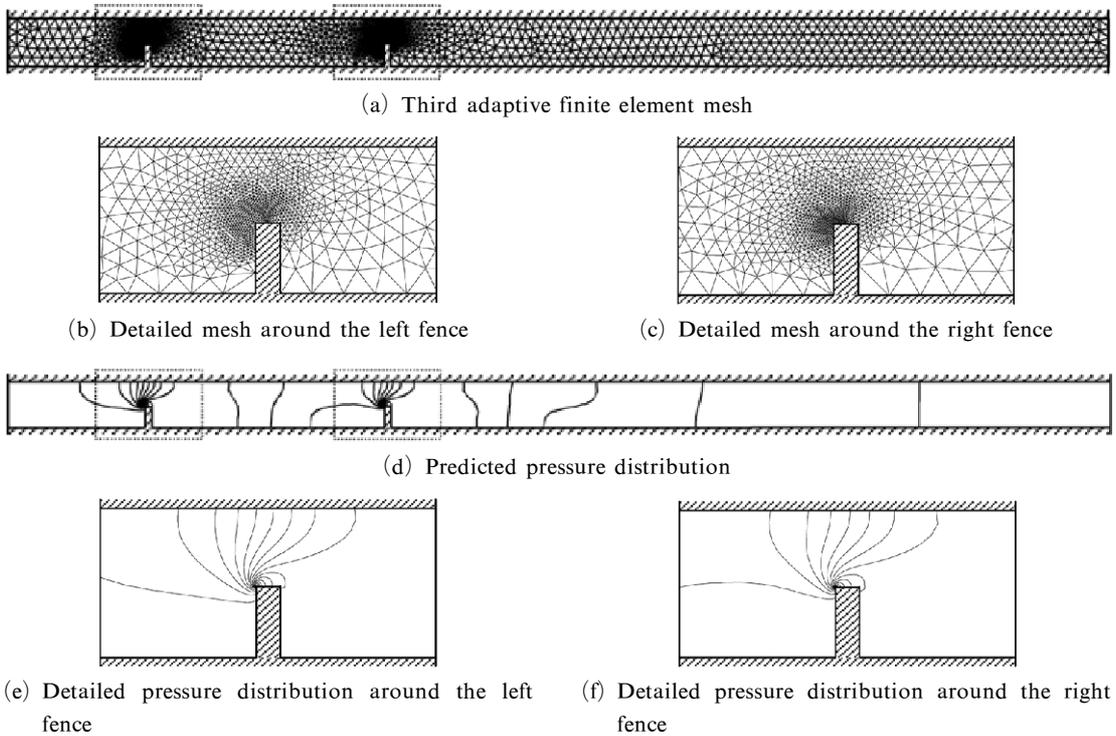(f) Detailed pressure distribution around the right fence

Fig. 16   Third adaptive mesh and its solution for flow past two fences in channel problem
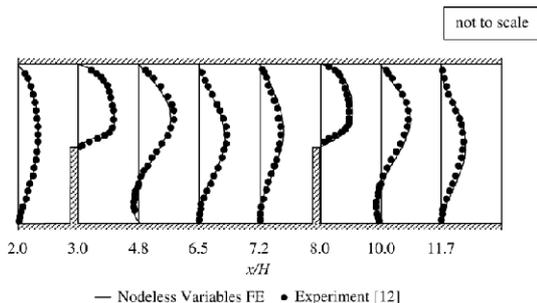
Fig. 17 Comparative velocity profiles for flow past two fences in channel

curacy as can be observed by the smooth pressure contours in Figs. 16(d) ~ (f). The predicted velocity profiles are compared with the experimental data (Durst et al., 1988) in Fig. 17. The figure shows good comparisons at different channel locations, with flow separations captured near the lower surface at x/H equals to 4.8 and 10.

7. Conclusions

The nodeless variables finite element method for viscous incompressible flow analysis was presented. The nodeless variables were incorporated into the standard three-node triangular elements to increase the order of the velocity interpolation functions. The nodeless variables finite elements avoid the need for using the six-node triangular elements normally employed to provide the analysis solution stability. The use of the nodeless variables finite elements reduces the difficulty for generating the meshes and provides modeling compatibility for the interdisciplinary analysis of coupled fluid/solid problems.

The nodeless variables finite element equations were derived from the governing Navier-Stokes differential equations. All finite element matrices were derived in closed-form and a corresponding computer program was developed. Two examples with exact and numerical solutions were used to validate the performance of the nodeless variables finite element method. The method was also combined with an adaptive meshing technique to further increase the overall analysis performance. The adaptive meshing technique generates small clustered elements in the regions of high solu-

tion gradients to increase the solution accuracy. Larger elements are generated in the other regions to reduce the computational time as well as the computer memory. The efficiency of the combined adaptive meshing technique and the nodeless variables finite element method was demonstrated by using the example of a flow past two fences in a channel.

References

Chen, X. and Han, P., 2000, "A Note on the Solution of Conjugate Heat Transfer Problems Using SIMPLE-Like Algorithm," *International Journal of Heat and Fluid Flow*, Vol. 21, pp. 463~467.

Dechaumphai, P. and Sikkhabandit, S., 2000, "Adaptive Finite Element Technique for Viscous Flow Analysis," *ASEAN Journal on Science and Technology for Development*, Vol. 17, No. 1, pp. 41~58.

Durst, F., Founti, M. and Obi, S., 1988, "Experimental and Computational Investigation of the Two-Dimensional Channel Flow over Two Fences in Tandem," *Trans. ASME, Journal of Fluids Engineering*, Vol. 110, pp. 48~54.

Kawahara, M., Yoshimura, N., Nakagawa, K. and Ohsaka, H., 1976, "Steady and Unsteady Finite Element Analysis of Incompressible Viscous Fluid," *International Journal of Numerical Methods in Engineering*, Vol. 10, pp. 437~456.

Limtrakarn, W. and Dechaumphai, P., 2004, "Interaction of High-Speed Compressible Viscous Flow and Structure by Adaptive Finite Element Method," *KSME International Journal*, Vol. 18, No. 10, pp. 1837~1848.

Patankar, S. V., 1980, *Numerical Heat Transfer and Fluid Flow*, McGraw-Hill, New York.

Ramaswamy, B. and Jue, T. C., 1991, "A Segregated Finite Element Formulation of Navier-Stokes Equations Under Laminar Conditions,"

Finite Element in Analysis and Design, Vol. 9, pp. 257~270.

Reddy, J. N. and Gartling, D. K., 1994, *The Finite Element Method in Heat Transfer and Fluid Dynamics*, CRC Press, Florida.

Schafer, M. and Teschauer, I., 2001, "Numerical Simulation of Coupled Fluid-Solid Problems," *Computer Methods in Applied Mechanics and Engineering*, Vol. 190, pp. 3645~3667.

Wansophark, N., Malatip, A. and Dechaumphai, P., 2005, "Streamline Upwind Finite Element Method for Conjugate Heat Transfer Problems," *To be Published in the Journal of Acta Mechanica Sinica*.

Yamada, Y., Ito, K., Yokouchi, Y., Tamano, T. and Ohtsubo, T., 1975, "Finite Element Analysis of Steady Fluid and Metal Flow," *Finite Element Methods in Fluids, Edited by Gallagher*, R. H., Zienkiewicz, O. C., Oden, J. T. and Taylor, C., Wiley, New York.

Zienkiewicz, O. C. and Taylor, R. L., 2000, *The Finite Element Method*, 5th Ed., Vol. 3, Fluid Dynamics, Butterworth-Heinemann, Oxford.